Mobility in excess of 10^6 cm^2/V s in InAs quantum wells grown on lattice mismatched InP substrates

A. T. Hatke, T. Wang, C. Thomas, G. C. Gardner, and M. J. Manfra

Citation: Appl. Phys. Lett. **111**, 142106 (2017);
View online: https://doi.org/10.1063/1.4993784
View Table of Contents: http://aip.scitation.org/toc/apl/111/14
Published by the American Institute of Physics

Mobility in excess of 10^6 cm^2/V s in InAs quantum wells grown on lattice mismatched InP substrates

A. T. Hatke,[1] T. Wang,[1,2] C. Thomas,[1,2] G. C. Gardner,[1,2,3] and M. J. Manfra[1,2,3,4]
[1]*Department of Physics and Astronomy and Station Q Purdue, Purdue University, West Lafayette, Indiana 47907, USA*
[2]*Birck Nanotechnology Center, Purdue University, West Lafayette, Indiana 47907, USA*
[3]*School of Materials Engineering, Purdue University, West Lafayette, Indiana 47907, USA*
[4]*School of Electrical and Computer Engineering and School of Materials Engineering, Purdue University, West Lafayette, Indiana 47907, USA*

(Received 30 June 2017; accepted 20 September 2017; published online 5 October 2017)

We investigate the transport properties of a two-dimensional electron gas residing in strained composite quantum wells of $In_{0.75}Ga_{0.25}As/InAs/In_{0.75}Ga_{0.25}As$ cladded with $In_{0.75}Al_{0.25}As$ barriers grown metamorphically on insulating InP substrates. By optimizing the widths of the $In_{0.75}Ga_{0.25}As$ layers, the $In_{0.75}Al_{0.25}As$ barrier, and the InAs quantum well, we demonstrate mobility in excess of 1×10^6 cm^2/V s. Mobility vs. density data indicate that scattering is dominated by a residual three dimensional distribution of charged impurities. We extract the effective Rashba parameter and spin-orbit length for these composite quantum wells. *Published by AIP Publishing.*
https://doi.org/10.1063/1.4993784

Due to a combination of strong spin-orbit coupling, large g-factor, and readily induced proximity superconductivity, the InAs based two-dimensional electron gas (2DEG) can support Majorana zero modes. A structure composed of a shallow InAs quantum well can be engineered to have proximity induced superconductivity with an *in-situ* epitaxial Al top layer with high transparency.[1] Such hybrid structures have been demonstrated to contain Andreev bound states that coalesce into Majorana zero modes[2,3] and are currently investigated as a promising platform for topological quantum computing.[1–7] While progress with the hybrid superconductor-shallow 2DEG system has been swift, fundamental limits to 2DEG transport properties imposed by metamorphic growth remain to be elucidated. To date, the maximum 2DEG mobility achieved on this system is $\mu \sim 6 \times 10^5$ cm^2/V s with 2DEG density $n \sim 6 \times 10^{11}$ cm^{-2} and parasitic conduction channels remain an issue.[8,9]

We investigate the limitations of the 2DEG mobility in the InAs quantum well on InP substrate system. Low temperature transport measurements are performed on gated Hall bars using symmetric $In_{0.75}Ga_{0.25}As/InAs/In_{0.75}Ga_{0.25}As$ quantum wells grown on (100) InP, where we vary the width of the flanking InGaAs layers, the depth of the quantum well from the surface, and the width of the InAs layer. While InAs has a 3.3% lattice mismatch to InP, the superior insulating property of Fe-doped InP substrates presents a crucial advantage for the measurement of high impedance devices necessary for the exploration of Majorana physics. Our results demonstrate record charge carrier mobility in excess of 1×10^6 cm^2/V s for this system and that our mobility appears to be limited by unintentional background charge impurities. We extract the Rashba parameter and spin-orbit length from the beating pattern of Shubnikov de-Haas oscillations (SdHOs). These results may be leveraged to improve the quality of InAs 2DEG structures used for topological quantum computing.

Our samples are grown using molecular beam epitaxy (MBE); see Ref. 10 for greater detail on how our MBE has been set up and maintained. The InAs structures are grown on semi-insulating InP (100) substrates that have been desorbed at 525 °C until a (2×3) to (2×4) surface phase transition is observed. First, a 100 nm thick $In_{0.52}Al_{0.48}As$ lattice matched smoothing layer upon which a $In_{0.52}Al_{0.48}As/In_{0.52}Ga_{0.48}As$ 2.5 nm five period superlattice is grown at 480 °C.[11] Due to a native lattice mismatch of 3.3% between InAs and InP, we grow a step graded buffer of $In_xAl_{1-x}As$ where $x = 0.52$ to 0.84 using 18 steps, 50 nm wide each, followed by a linearly ramped reverse step from $x = 0.84$ to 0.75 to relieve any residual strain. The graded buffer layer and reverse step are grown at 360 °C.

The active region comprising the composite quantum well plus barriers is then grown. The substrate temperature is increased to 480 °C to grow a 25 nm $In_{0.75}Al_{0.25}As$ bottom barrier and active region composed of a strained $w = 4$ nm ($w = 6$ nm for Sample E only) InAs layer flanked on either side by symmetric $In_{0.75}Ga_{0.25}As$ layers to promote higher mobility.[12,13] For Samples A, B, and C, we vary only the width of the $In_{0.75}Ga_{0.25}As$ layers to be $d = 5$, 10.5, and 15 nm, respectively. The sample growth is completed with a $b = 120$ nm ($b = 180$ nm for Sample D only) $In_{0.75}Al_{0.25}As$ top barrier to remove the active region from the surface and minimize anisotropy effects that can become apparent when the active region of the quantum well is to near the surface.[14,15] Finally, we do not include an InGaAs capping layer to avoid the formation of a parallel conduction channel[9] or intentional doping. In the inset of Fig. 1, we schematically depict the layer stack for the active region. A summary of the five samples discussed here is presented in Table I. We note that all samples have a nominal as-grown 2DEG density $n \sim 5 \times 10^{11}$ cm^{-2}. As the structures are not intentionally modulation doped, the carriers must originate from donor-like states distributed in the epilayers. The precise density and distribution of native and unintentionally incorporated impurity donor-like defects are not currently known. Native defects are expected to be more numerous in the graded

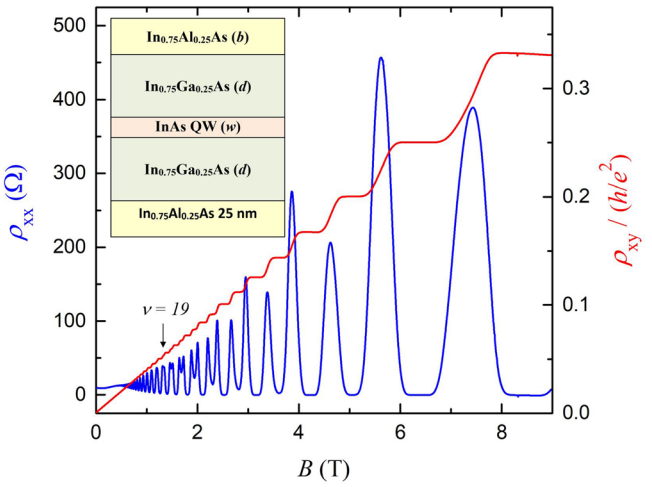

FIG. 1. Longitudinal, ρ_{xx}, and Hall, ρ_{xy} normalized to h/e^2 (inverse filling factor), resistivities vs. magnetic field, B, for density $n = 6.2 \times 10^{11}\,\mathrm{cm}^{-2}$, left and right axis respectively, for Sample B. Inset: Schematic representation of the layer stack for the active region of the quantum well; see text for greater detail.

buffer region where relaxation of the lattice constant towards InAs is accompanied by defect generation.

Our samples are processed with standard wet etching techniques to define both straight and L-shaped (aligned along the $[1\bar{1}0]$ and [110] directions) Hall bars of width $w = 150\,\mu$m. After etching, we deposit Ti/Au ohmic contacts of thickness 80/250 nm, a 40 nm Al_2O_3 dielectric using thermal atomic layer deposition, and a 20/150 nm Ti/Au gate. All samples have a zero gate voltage, $V_G = 0$, density of $n = 5.3$–$5.6 \times 10^{11}\,\mathrm{cm}^{-2}$ with Δn versus V_G in good agreement with a simple capacitance model. The samples were measured in a ^{3}He system at a base temperature of $T = 300$ mK using standard low frequency lockin techniques with an excitation current of 0.5 μA.

InAs quantum wells based on GaSb substrates with $Al_{0.37}Ga_{0.67}Sb$ barriers[16] have recently been shown to achieve mobilities of $\mu = 2.4 \times 10^6\,\mathrm{cm}^2/\mathrm{V\,s}$ at $n \sim 1 \times 10^{12}\,\mathrm{cm}^{-2}$.[17] The sample structures investigated here are instead grown on lattice mismatched InP substrates that have superior insulating properties, a requirement when operating mesoscopic devices in high resistance configurations. The highest reported mobility for such a structure is $\mu = 0.6 \times 10^6\,\mathrm{cm}^2/\mathrm{V\,s}$ achieved at $n \sim 5 \times 10^{11}\,\mathrm{cm}^{-2}$,[9] but supporting transport data were not provided.

We begin our discussion with Sample B, which yielded the highest mobility. In Fig. 1, we present longitudinal (ρ_{xx}, left axis) and Hall (ρ_{xy} normalized to h/e^2, right axis) resistivities versus magnetic field (B) for $n = 6.2 \times 10^{11}\,\mathrm{cm}^{-2}$.

TABLE I. Sample details for dimensions of the top $In_{0.75}Al_{0.25}As$ barrier layer, the symmetric $In_{0.75}Ga_{0.25}As$ layers, and the InAs quantum well width.

	$In_{0.75}Al_{0.25}As$ (nm)	$In_{0.75}Ga_{0.25}As$ (nm)	InAs (nm)
Sample A	$b = 120$	$d = 5$	$w = 4$
Sample B	$b = 120$	$d = 10.5$	$w = 4$
Sample C	$b = 120$	$d = 15$	$w = 4$
Sample D	$b = 120$	$d = 10.5$	$w = 6$
Sample E	$b = 180$	$d = 10.5$	$w = 4$

We observe the absence of a parasitic parallel conduction channel from the linear low field ρ_{xy}. There is also good agreement between the extracted density from both the Hall slope and the period of Shubnikov de-Haas oscillations (SdHOs). With increasing B we observe a spin splitting onset at filling factor $\nu = nh/eB = 19$, where h is the Planck constant and e is the electron charge, as marked in Fig. 1, with well developed integer quantum Hall states, $\rho_{xx} = 0$ and $\rho_{xy} = Nh/e^2\nu$, where N is an integer.

We continue with Sample B with gating to obtain μ versus n, as shown in Fig. 2(a), for a straight Hall bar aligned along the $[1\bar{1}0]$ direction. A maximum mobility of $\mu = 1.1 \times 10^6\,\mathrm{cm}^2/\mathrm{V\,s}$ occurs at $n = 6.2 \times 10^{11}\,\mathrm{cm}^{-2}$. This is the largest reported μ for an InGaAs/InAs/InGaAs quantum well. On a device processed during a different fabrication, from the same wafer as Sample B, we plot μ versus n where measurements were performed on an L-shaped Hall bar in Fig. 2(b). The gating dependence shows that there is minimal anisotropy between the $[1\bar{1}0]$ and [110] directions with less than 5% difference. Thus, we compare samples only along the $[1\bar{1}0]$ direction for the remainder of the manuscript.

To determine what limits mobility in our structure, we assume the μ versus n dependence can be described by a simple power law, $\mu \propto n^{\alpha}$, and extract the exponent α, using a log-log plot (not shown) giving equal weight to all data, in the restricted density range of $n > 1.5 \times 10^{11}\,\mathrm{cm}^{-2}$. In this high 2DEG density and strong screening limit $q_{TF} \gg k_F$, where q_{TF} is the Thomas-Fermi wave vector,[18] α will approach two values: for the case of unintentional background impurities $\alpha \to 1/2$, however, when scattering is dominated by remote two-dimensional impurities

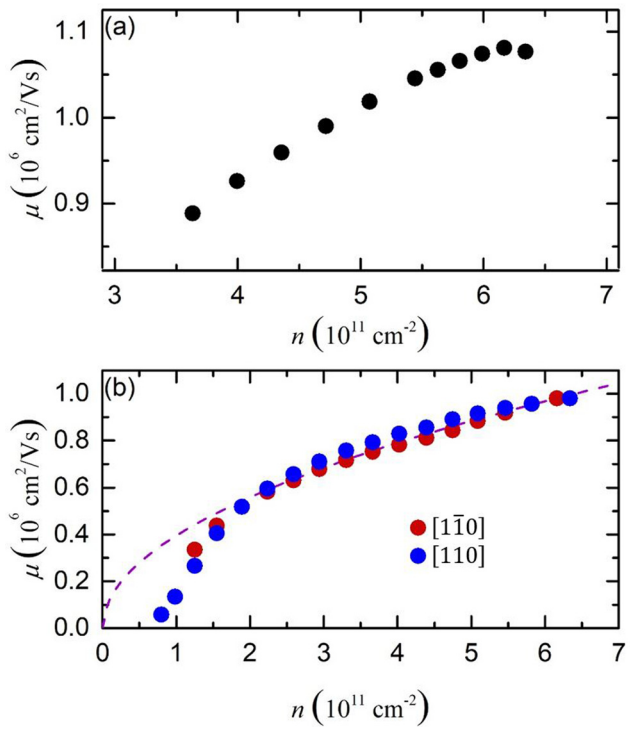

FIG. 2. Mobility vs. density, μ vs. n: (a) Sample B on a straight Hall bar oriented along the $[1\bar{1}0]$ direction demonstrating a peak mobility of $\mu = 1.1 \times 10^6\,\mathrm{cm}^2/\mathrm{V\,s}$ at $n = 6.2 \times 10^{11}\,\mathrm{cm}^{-2}$. (b) Sample B obtained from an L-shaped Hall bar along the two main crystallographic directions and a fit line to $\mu \propto n^{\alpha}$ where $\alpha = 0.5$.

$\alpha \rightarrow 3/2$.[19] In Fig. 2(b), the extracted fit, dashed line, for $\alpha = 0.5$ fits well over the density range of interest and is roughly equivalent for all samples measured in this study. This indicates that the mobility is limited by unintentional background impurities and native charged point defects.[19]

In Ref. 20, a similar structure was investigated that contained 8 nm $In_{0.75}Ga_{0.25}As$ layers where $\alpha \sim 0.8$ was observed. It appears that mobility in the structures of Ref. 20 and those of our own work is largely dominated by background impurity scattering.[19] As mobility scales linearly with the density of charged background defects, the higher peak mobility observed here may be attributed to differences in background defect concentration. The slight difference in α may be attributed to variations in the scattering center density distribution along the growth axis. We expect that the density of unintentionally incorporated impurity atoms is likely to be low in our material. We have grown AlGaAs/GaAs two-dimensional electron gases in the same system with mobility in excess of 1×10^7 cm^2/V s during the same growth campaign. This places limits on the uniformly distributed charged impurity density $\leq 10^{14}$ cm^{-3} for the well understood and characterized AlGaAs/GaAs system grown in the same MBE chamber.[21] Thus, even if we allow for background scatters (native and impurity defects) with a density of 10^{15} cm^{-3} in our InAs structures (a factor of 10 higher than for GaAs), the limit to mobility still is only approximately 3×10^6 cm^2/V s when one accounts for the nearly factor of 3 difference in the effective mass between InAs and GaAs.[21] The identification of the precise location and density of charged defects in our epilayers is the subject of ongoing research beyond the scope of this paper.

Alloy scattering and interface roughness will also act to limit mobility at low temperatures. In hybrid InGaAs/InAs/InGaAs quantum wells studied here, the self-consistent Schrodinger-Poisson calculations show that the electron wavefunction is confined primarily in the pure InAs layer ($\geq 53\%$ for the highest mobility structure). This localization in the InAs layer reduces the effective carrier mass, reducing the impact of background impurity scattering on mobility, and reduces the impact of alloy scattering when compared to uniform random alloy $In_{0.75}Ga_{0.25}As$ quantum wells.[8,22] Galiev *et al.*[23] reported an $\sim 1.5\times$ increase of mobility at $T = 77$ K upon insertion of a 4 nm InAs layer into an $In_{0.53}Ga_{0.47}As$ quantum well holding all other parameters constant.

The impact of changes to a heterostructure design is evaluated using zero-field mobility as the metric. We investigate perturbations to Sample B beginning with the well width dependence of the $In_{0.75}Ga_{0.25}As$ layers. In Fig. 3(a), we plot μ versus n for Samples A–C where the $In_{0.75}Ga_{0.25}As$ layer widths are $d = 5$, 10.5, and 15 nm, respectively. For Sample C, $d = 15$ nm, there is a nonmonotonic μ versus n where μ begins to decrease for $n > 4.25 \times 10^{11}$ cm^{-2}. This nonmonotonic n-dependence is due to occupation of the second subband. Estimation of the onset density of the second subband becoming populated occurs at $n \sim 7.5$, 6, and 5×10^{11} cm^{-2} for Samples A–C, respectively, from the self consistent calculations performed with Nextnano.[3,24]

At fixed n, there is a nonmonotonic dependence of μ versus d. At $n \sim 4 \times 10^{11}$ cm^{-2}, for example, $\mu = 0.83 \times 10^6$ cm^2/V s for $d = 10.5$ nm, that decreases to $\mu = 0.73 \times 10^6$ cm^2/V s

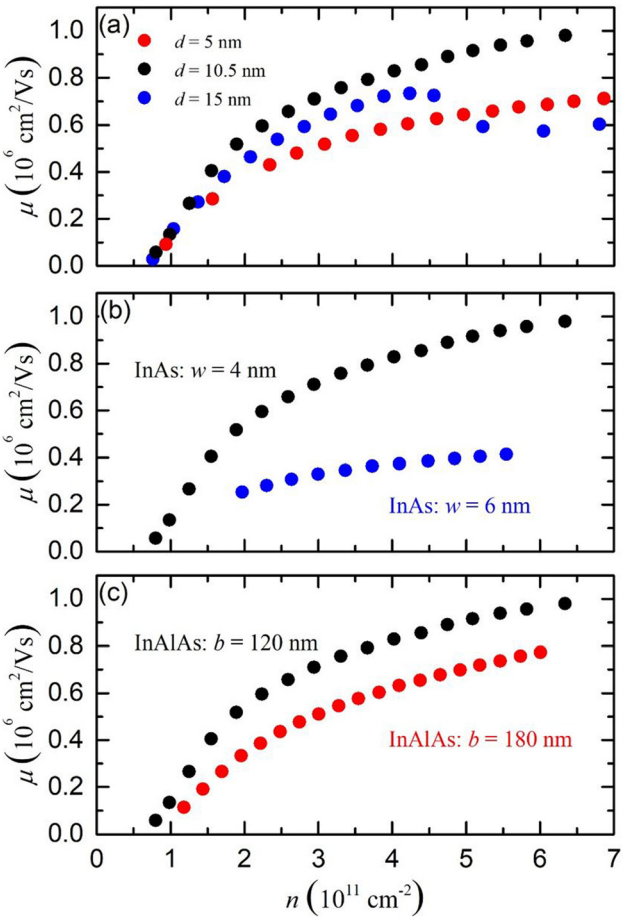

FIG. 3. μ vs. n: (a) Comparison from Samples A–C where the width, d, of the InGaAs layer is varied. (b) Comparison between Samples B and D where the width, w, of the InAs quantum well is varied. (c) Comparison between Samples B and E where the width, b, of the top InAlAs barrier is varied.

and $\mu = 0.59 \times 10^6$ cm^2/V s for $d = 15$ and 5 nm, respectively. With a large overlap in the sample structure between the three samples, we do not expect changes in scattering from background impurities, remote impurities, or charged dislocations to be responsible for the observed width dependence. Increasing d results in a spread of the charge distribution such that there is an increase of the amount of charge that resides in the $In_{0.75}Ga_{0.25}As$ layers. An increase of the amount of wavefunction extension into the $In_{0.75}Ga_{0.25}As$ layer will decrease the mobility due to an increase in the amount of alloy scattering. The decrease of μ of $\sim 12\%$ is due to a $\sim 1\%$ transfer of charge from the pure InAs to the $In_{0.75}Ga_{0.25}As$ layer implies a strong dependence on alloy scattering. A more dramatic reduction in the mobility occurs when there is a decrease of d, which can come from two sources: (1) alloy scattering and (2) interface scattering. The charge distribution in the effective 14 nm well of Sample C will penetrate into the $In_{0.75}Al_{0.25}As$ barriers giving an increased amount of alloy scattering, as observed in Nextnano[24] simulations. Additionally, the increased confinement of the charge results in an increase in scattering at the $In_{0.75}Ga_{0.25}As$/InAs interface. The comparison of the integrated charge density of the wells of Samples B and C in a restricted region of 0.5 nm to either side of the InGaAs/InAs interface shows that the amount of charge in the region of the interface increases giving rise to increased interface scattering.

In Fig. 3(b), μ versus n for Samples B and D where the width of the InAs quantum well is increased from $w = 4$ to 6 nm is plotted. A large reduction in μ throughout the entire n-range for $w = 6$ nm is observed. Naively, one might expect μ to increase with an increase in w, as a larger percentage of the charge density would reside in the InAs part of the well resulting in a decrease in alloy scattering from the $In_{0.75}Ga_{0.25}As$ layers. However, the severe reduction in μ implies that the critical thickness, w_c, of the InAs has been exceeded which introduces misfit dislocations to the quantum well.[9,25] We estimate $w_c \sim 5.5$ nm, for this In concentration.

In Fig. 3(c), μ versus n is plotted for Samples B and E where the $In_{0.75}Al_{0.25}As$ barrier is changed from $b = 120$ to 180 nm, respectively. Again, there is an overall decrease in μ. As previously discussed, μ is limited by background charged impurities which suggests that while b is increased in Sample E to reduce surface effects the possible gain is compensated by the increased level of charged impurities introduced by the additional $In_{0.75}Al_{0.25}As$ layers resulting in decreased μ.

We preformed further measurements of Sample B at low B to investigate the spin-orbit coupling. In Fig. 4(a), we plot the oscillatory correction to the magnetoresistivity, $\Delta\rho_{xx}$, for $n = 5.1 \times 10^{11}\,\mathrm{cm}^{-2}$ after removal of a slowly varying background. With increasing B, we observe the onset of SdHOs at $B \sim 0.2$ T and this low B value is another indication of the high quality of the 2DEG. The amplitude of the SdHOs increases with increasing B but demonstrates a beating pattern with a node at $B \sim 0.3$ T. By restricting our analysis to densities below the occupation of the second subband, this beating pattern can be ascribed to two oscillation periods that are nearly equal and has been demonstrated in these structures to arise from zero field spin splitting between slightly different spin up and spin down densities.[26–28]

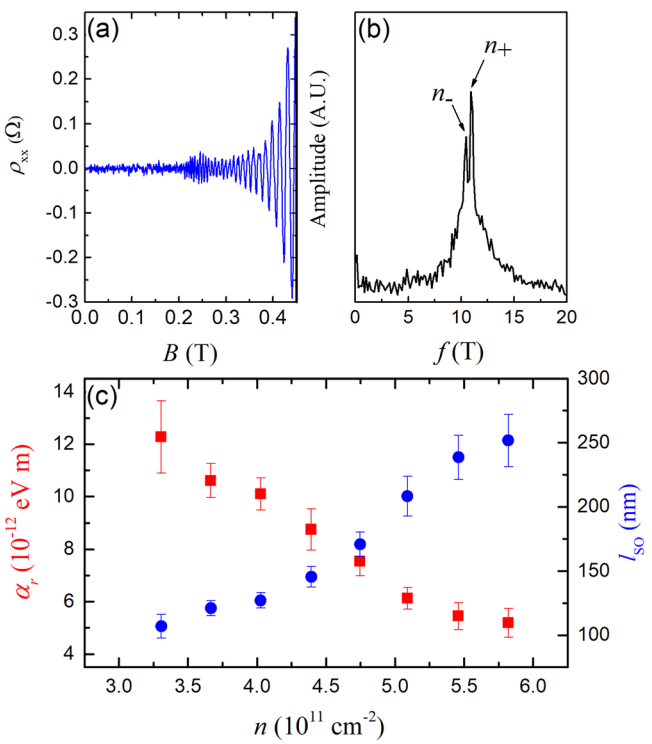

FIG. 4. (a) Low field magnetoresistivity with the removal of a smoothly varying background, $\Delta\rho_{xx}$ vs. B, for $n = 5.1 \times 10^{11}\,\mathrm{cm}^2$ on Sample B. (b) Amplitude of an FFT of ρ_{xx} from inverse B. (c) Rashba parameter, α_r squares, and spin orbit length, ℓ_{SO} circles, vs. n, left and right axis, respectively.

In Fig. 4(b), we present the amplitude of the fast Fourier transform (FFT) versus frequency of the magnetotransport after conversion to inverse magnetic field. This FFT split peak can be assigned to two spin-split subbands with densities n_+ and n_-, which can be calculated from $n_\pm = ef/h$. From this assignment, the estimated total density $n_T = n_+ + n_-$ is in good agreement with that obtained from the Hall slope and the SdHO minima period.

In systems that lack inversion symmetry, the dominant source of spin-orbit interaction is due to the Rashba effect, which arises from an electric field perpendicular to the plane of the 2DEG. This electric field can be a result of an inversion asymmetry built into the system based on the 2DEG design or from an applied field from a gate.[29] From the SdHO beating pattern, we extract the Rashba parameter $\alpha_r = \frac{\Delta n \hbar^2}{m^*}\sqrt{\frac{\pi}{2(n_T - \Delta n)}}$, where $\Delta n = n_+ - n_-$ and we assume $m^* = 0.03$.[20] We perform FFTs at different V_G and extract α_r versus n in Fig. 4(c), left axis. The Rashba effect is due to an asymmetry in the azimuthal direction and is proportional to the electric field, $\alpha_r = \alpha_0\langle E_z\rangle$, where α_0 is a material specific parameter. Our gating density dependence is very nearly linear and follows from the simple capacitance model, where we observe a linear change to n so we expect a linear increase of α_r with decreasing n, corresponding to an increase in E_Z. The values we obtain for α_r are of the same order as those obtained from InAs systems with symmetric Si doping,[27] built in $In_{0.53}Ga_{0.47}As$ layer asymmetry,[28,30,31] or those reported with AlSb barriers.[16]

To eliminate effective mass dependence, we recast α_r as the spin-orbit length, $\ell_{SO} = \frac{1}{\Delta n}\sqrt{\frac{n_T - \Delta n}{2\pi}}$, versus n and plot the result in Fig. 4(c), right axis. Physically, the spin-orbit length gives a measure of the average distance traversed by an electron before a spin flip occurs. In the case of weak spin-orbit interaction, the high n (low V_G) case, the spin will travel further through the system, larger ℓ_{SO}, before its spin orientation will become essentially randomized. With the increase of the spin-orbit interaction under applied gate voltage, the electron traverses decreasing distance before its spin is randomized.

This research was supported by Microsoft Station Q.

[1]J. Shabani, M. Kjaergaard, H. J. Suominen, Y. Kim, F. Nichele, K. Pakrouski, T. Stankevic, R. M. Lutchyn, P. Krogstrup, R. Feidenhans'l *et al.*, Phys. Rev. B **93**, 155402 (2016).
[2]H. J. Suominen, M. Kjaergaard, A. R. Hamilton, J. Shabani, C. J. Palmstrom, C. M. Marcus, and F. Nichele, e-print arXiv:1703.03699.
[3]F. Nichele, A. C. C. Drachmann, A. M. Whiticar, E. C. T. O'Farrell, H. J. Suominen, A. Fornieri, T. Wang, G. C. Gardner, C. Thomas, A. T. Hatke *et al.*, Phys. Rev. Lett. **119**, 136803 (2017).
[4]S. D. Sarma, M. Freedman, and C. Nayak, Phys. Rev. Lett. **94**, 166802 (2005).
[5]J. Alicea, Y. Oreg, G. Refael, F. von Oppen, and M. P. A. Fisher, Nat. Phys. **7**, 412 (2011).
[6]M. Kjaergaard, F. Nichele, H. J. Suominen, M. P. Nowak, M. Wimmer, A. R. Akhmerov, J. A. Folk, K. Flensberg, J. Shabani, C. J. Palmstrom *et al.*, Nat. Commun. **7**, 12841 (2016).
[7]M. Kjaergaard, H. J. Suominen, M. P. Nowak, A. R. Akhmerov, J. Shabani, C. J. Palmstrom, F. Nichele, and C. M. Marcus, Phys. Rev. Appl. **7**, 034029 (2017).

[8]S. Gozu, T. Kita, Y. Sata, S. Yamada, and M. Tomizawa, J. Cryst. Growth **227–228**, 155 (2001).
[9]J. Shabani, A. P. McFadden, B. Shojaei, and C. J. Palmstrom, Appl. Phys. Lett. **105**, 262105 (2014).
[10]G. C. Gardner, S. Fallahi, J. D. Watson, and M. J. Manfra, J. Cryst. Growth **441**, 71 (2016).
[11]C. Heyn, S. Mendach, S. Lhr, S. Beyer, S. Schnll, and W. Hansen, J. Cryst. Growth **251**, 832 (2003).
[12]M. Sexl, G. Bohm, D. Xu, H. Heib, S. Kraus, G. Trankle, and G. Weimann, J. Cryst. Growth **175–176**, 915 (1997).
[13]X. Wallart, J. Lastennet, D. Vignaud, and F. Mollot, Appl. Phys. Lett. **87**, 043504 (2005).
[14]A. Richter, M. Koch, T. Matsuyama, C. Heyn, and U. Merkt, Appl. Phys. Lett. **77**, 3227 (2000).
[15]S. Lohr, S. Mendach, T. Vonau, C. Heyn, and W. Hansen, Phys. Rev. B **67**, 045309 (2003).
[16]B. Shojaei, A. C. C. Drachmann, M. Pendharkar, D. J. Pennachio, M. P. Echlin, P. G. Callahan, S. Kraemer, T. M. Pollock, C. M. Marcus, and C. J. Palmstrom, Phys. Rev. B **94**, 245306 (2016).
[17]T. Tschirky, S. Mueller, C. A. Lehner, S. Falt, T. Ihn, K. Ensslin, and W. Wegscheider, Phys. Rev. B **95**, 115304 (2017).
[18]F. Stern, Phys. Rev. Lett. **18**, 546 (1967).
[19]S. D. Sarma and E. H. Hwang, Phys. Rev. B **88**, 035439 (2013).
[20]J. Shabani, S. D. Sarma, and C. J. Palmstrom, Phys. Rev. B **90**, 161303 (2014).
[21]E. H. Hwang and S. D. Sarma, Phys. Rev. B **77**, 235437 (2008).
[22]C. Chen, I. Farrer, S. N. Holmes, F. Sfigakis, M. P. Fletcher, H. E. Beere, and D. Ritchie, J. Cryst. Growth **425**, 70 (2015).
[23]G. B. Galiev, I. S. Vasil'evskii, E. A. Klimov, S. S. Pushkarev, A. N. Klochkov, P. P. Maltsev, M. Y. Presniakov, I. N. Trunkin, and A. L. Vasiliev, J. Mater. Res. **30**, 3020 (2015).
[24]See http://www.wsi.tum.de/nextnano3 and http://www.nextnano.de for The Nextnano software.
[25]F. Capotondi, G. Biasiol, D. Ercolania, and L. Sorba, J. Cryst. Growth **278**, 538 (2005).
[26]S. Datta and B. Das, Appl. Phys. Lett. **56**, 665 (1990).
[27]K.-H. Kim, H. Kim, H. C. Koo, J. Chang, and S.-H. Han, Appl. Phys. Lett. **97**, 012504 (2010).
[28]T. Y. Lee, J. Chang, M. C. Hickey, H. C. Koo, H.-J. Kim, S. H. Han, and J. S. Moodera, Appl. Phys. Lett. **98**, 202504 (2011).
[29]J. Nitta, T. Akazaki, H. Takayanagi, and T. Enoki, Phys. Rev. Lett. **78**, 1335 (1997).
[30]T. Schpers, J. Knobbe, A. van der Hart, and H. Hardtdegen, Sci. Technol. Adv. Mater. **4**, 19 (2003).
[31]Y. H. Park, H. J. Kim, J. Chang, S. H. Han, J. Eom, H.-J. Choi, and H. C. Koo, Appl. Phys. Lett. **103**, 252407 (2013).